Isotope effect in transient electron thermal transport property and its impact on the electron internal transport barrier formation in LHD

T. Kobayashi[1,2], K. Ida[1], K. Tanaka[1], M. Yoshinuma[1], T. Ii Tsujimura[1], S. Inagaki[3,4], T. Tokuzawa[1], H. Tsuchiya[1], N. Tamura[1], H. Igami[1], Y. Yoshimura[1], S.-I. Itoh[4,3,5,†], K. Itoh[6,1,4] and LHD Experiment Group

[1] National Institute for Fusion Science, National Institutes of Natural Sciences, Toki 509-5292, Japan

[2] The Graduate University for Advanced Studies, SOKENDAI, Toki 509-5292, Japan

[3] Research Institute for Applied Mechanics, Kyushu University, Kasuga 816-8580, Japan

[4] Research Center for Plasma Turbulence, Kyushu University, Kasuga 816-8580, Japan

[5] Graduate School of Engineering, Chubu University, Kasugai 487-8501, Japan

[6] Institute of Science and Technology Research, Chubu University, Kasugai 487-8501, Japan

[†] Deceased July 18, 2019

E-mail: kobayashi.tatsuya@nifs.ac.jp

Abstract. In this study, we perform a comprehensive comparison of the transport hysteresis width in deuterium (D) plasmas, hydrogen (H) plasmas, and D-H mixed plasmas. The core focused modulation electron cyclotron resonance heating (MECH) is applied as the heat source perturbation, and the heat flux is evaluated using the energy conservation equation with the measured electron temperature response and the ECH deposition profile calculated by the ray-tracing scheme. Systematic density scan in plasmas with different ion mass reveals that there is no significant isotope effect in their hysteresis width. It is found that plasmas with heavier isotope mass can easily form the electron internal transport barrier. As the hysteresis width is

insensitive to the isotope mass, the classical part of the diffusivity is considered to be responsible for the isotope effect in the transport barrier formation.

1. Introduction

One of the long-standing mysteries in magnetically confined fusion plasma research is the hydrogen isotope effect [1, 2, 3, 4, 5]. In the simplest scaling model, i.e., the Bohm scaling model or the gyro-Bohm scaling model [6, 7, 8], it is predicted that the heavier the fuel particles are the worse the confinement becomes. However, the experimental investigations showed the opposite tendency. Many of these studies were based on the transport analysis using the steady state confinement time or the power balance diffusivity. As another technique, the thermal transport property can be analyzed from the plasma response with respect to a fractional perturbation applied on the heating source, which we call the transient transport analysis [9, 10, 11]. It is known that the transport coefficients obtained by the power balance analysis and by the transient transport analysis differ when nonlinearities exist in the flux-gradient relation, e.g., the critical gradient [10, 11, 12, 13]. All of these analyses implicitly assume that the plasma thermal transport is uniquely determined by the local plasma parameters.

However, some counter examples for those local transport models have been reported in particular when the plasma heat source or sink are subject to transient perturbations, e.g., by the local and intense electron heating [14, 15, 16, 17, 18, 19] or by the edge plasma cooling [20, 21, 22]. These phenomena are called the nonlocal

thermal transport [23], and considered to be of great importance for predicting future reactor performance [24]. Recently, a direct impact of the heating source on the plasma turbulence and thus on the turbulent transport was experimentally pointed out [18, 19]. Because of this ingredient, the turbulence amplitude is allowed to change immediately after an additional heat source is applied and before the local parameters change. This response results in the bifurcation of the trajectory in the flux–gradient diagram depending on the applied ECH power [25, 26, 27]. In particular, under a modulation ECH (MECH) application, the trajectory in the flux–gradient diagram draws a loop, which we call the transport hysteresis. When the transport hysteresis emerges, a single scalar transport coefficient is found to be no longer valid for representing the transport property of the high temperature plasmas [28, 29, 30, 31]. A theoretical model predicts that the magnitude of the hysteresis is more enhanced in lighter isotope mass plasmas, which results in the confinement degradation and therefore explains the isotope effect [27].

To date, there are few experimental assessments for the isotope effect on the transient thermal transport such as the transport hysteresis. In this study, in addition to the recent phenomenological investigations for the heating power dependence [18] or the density dependence [19] of the hysteresis width, we perform a comprehensive comparison of the transport hysteresis width in deuterium (D) plasmas, hydrogen (H) plasmas, and D-H mixed plasmas. The core focused MECH is applied as the heat source perturbation, and the heat flux is evaluated using the energy conservation equation with

the measured electron temperature response and the ECH deposition profile calculated by the ray-tracing scheme. Systematic density scan in plasmas with different ion mass reveals that there is no significant isotope effect in their hysteresis width. In the low density plasmas, the internal transport barriers (ITBs) [32] are dynamically formed in the electron temperature profile with the MECH. It is found that plasmas with heavier isotope mass can form ITBs with higher density at a fixed heating power similar to the case of ITBs in the ion temperature profile [33]. As the hysteresis width is insensitive to the isotope mass, the classical part of the diffusivity is considered to be essential for the isotope effect in the density threshold of the ITB.

This paper is organized as follows. Section 2 is dedicated to a brief review of the hysteresis study, in which the detailed analysis technique and the theoretical background are exhibited. The experimental setup is given in section 3, and the experimental results appear in section 4. As an interpretation of the results, a theoretical model involving the direct impact of the heat source modulation on turbulence is examined in section 5. At last, the paper is summarized in section 6.

2. A brief review of transport hysteresis

For describing the thermal transport property in plasma, a number of theoretical models have been developed so far. One of the most commonly used models is the local diffusion–convection model [10]. An advantage of this model is that the transport can be expressed only by two scalar coefficients, i.e., the diffusivity and the convective

velocity. However, if the assumed model is improper in accounting for the actual plasma transport, obtained results immediately mislead us in interpreting the plasma thermal confinement [28, 29, 30]. To prevent overlooking phenomena outside the assumed model, we prefer to directly observe the flux–gradient relation.

Spatiotemporal evolution of the electron heat flux perturbation $\tilde{q}_{\rm e}(t,r)$ induced by the heating source modulation $\tilde{P}(r,t)$ can be obtained by the energy conservation equation as

$$\tilde{q}_{\rm e}(t,r) = \frac{1}{V'(r)} \int_0^r \left[\tilde{P}(r,t) - \frac{3}{2} n_{\rm e}(r,t) \frac{\partial \tilde{T}_{\rm e}(r,t)}{\partial t} \right] V'(r) dr, \tag{1}$$

where $V'(r)$ is the radial derivative of the plasma volume profile [18, 19]. Data in different modulation periods are regarded as independent realizations, which are subject to the conditional ensemble averaging for reducing the statistical noise. By drawing obtained $\tilde{q}_{\rm e}(t,r)$ as a function of the local electron temperature gradient, the flux–gradient relation is obtained.

By performing the flux–gradient relation analysis, the transport hysteresis was found [18, 19]. The typical transport hysteresis is illustrated in Fig. 1 [27, 34, 35]. There are two different dynamics in the heat flux evolution having fast and slow time constants. When the ECH is turned on, the heat flux increases with a fast time scale and a slight change in the electron temperature gradient. It is followed by the heat flux evolution with a slow time constant, which is well approximated by the local diffusion model. When the ECH is turned off, a fast drop of the heat flux occurs. Consequent slow decreases in the heat flux and the local electron temperature gradient finally close

the trajectory as a parallelogram loop. Here, the peak-to-peak variations in the heat flux and in the electron temperature gradient at a single modulation of the heat source are denoted as $\delta q_{\rm ECH}$ and $-\delta\nabla T_{\rm e}$, respectively. The magnitude of the heat flux "jump" at the fast time scale immediately after the ECH turn-on or turn-off is expressed as $\delta q_{\rm jump}$. The entire heat flux is therefore modeled as

$$q_{\rm e} = -n_{\rm e}\chi_{\rm e}^{\rm Slow}\nabla T_{\rm e} + \delta q_{\rm jump}, \tag{2}$$

where $\chi_{\rm e}^{\rm Slow}$ is the slow time scale diffusivity. Since the variation in the electron temperature gradient at the fast time scale dynamics is negligibly small, $\chi_{\rm e}^{\rm Slow}$ is approximated as

$$\chi_{\rm e}^{\rm Slow} \sim -(\delta q_{\rm ECH} - \delta q_{\rm jump})/n_{\rm e}\delta\nabla T_{\rm e}. \tag{3}$$

Here, the electron density is treated to be constant in time during the MECH according to the experimental observation. In this diagram, the heat pulse diffusivity $\chi_{\rm e}^{\rm HP}$ corresponds to the slope of a diagonal connecting the left bottom and the right top. When $\delta q_{\rm jump}$ is absent, $\chi_{\rm e}^{\rm Slow}$ is equivalent to $\chi_{\rm e}^{\rm HP}$ and the local diffusion model holds.

At the moment of the ECH turn-on or turn-off, the heat flux drastically changes with a tiny change in the local electron temperature gradient. This is the typical feature of the nonlocal transport, i.e., flux variation not driven by the local gradient. Here, the contribution of the off-diagonal terms in the transport matrix is also excluded since any local parameter cannot vary in such a fast time scale. Theoretically, this fast nonlocal response is modeled to be an enhanced turbulent fluctuation directly driven by the applied heat source. In other words, the applied heat source is regarded as a "hidden

parameter", which induces the bifurcation in the flux–gradient relation. The direct impact of the heat source on the turbulence is also considered to be strongly related to the power degradation of the thermal transport [36, 37]. As a different example of the "hidden parameter" in the flux–gradient relation, the electron density gradient is claimed to be responsible for the nonlocal cold pulse propagation by only using an off-diagonal local transport model [38, 39, 40].

3. Experimental setup

The set of MECH experiments was performed in the 20th experimental campaign of the Large Helical Device (LHD). The magnetic axis and the toroidal magnetic field in the vacuum configuration are $R_{\rm ax} = 3.6$ m and $B_{\rm t} = 2.75$ T, respectively. The plasma minor radius is defined by the effective minor radius in which 99 % of the plasma kinetic energy is confined, to be $a_{99} \sim 0.6$ m. The plasma is sustained by two tangential neutral beams (NBs) injected in the balanced manner to prevent the NB driven plasma current. The MECH focused on the core is superposed on it to study the heat pulse electron thermal transport. The electron temperature perturbation is measured by the electron cyclotron emission (ECE) radiometer [41], whose intensity is calibrated by the electron temperature data measured by the Thomson scattering [42]. The ECH deposition profile is calculated by the ray-tracing code LHDGauss [43].

It was demonstrated that the hysteresis width strongly depends on the line averaged electron density [19]. We refrain to make a one-by-one comparison of plasmas with

Table 1. List of dataset used in the transient transport analysis

Date of experiment	Shot numbers	Gas puff	Beam source
November 28, 2018	146808–146824	D	D
December 7, 2018	147880–147883	H	D
February 8, 2019	152210–152237	H	H

different isotope contents to avoid an imperfect match of the density, which could provide an ambiguity to the results. Instead, the line averaged density dependences of the hysteresis width in D, H and D-H mixed plasmas are compared.

Table 1 summarizes the date of experiment, the shot number, and the plasma fuel gases. Because the target plasmas are NB produced, not only the gas puff but also the beam fueling impacts the plasma ion purity. The experiments on November 28, 2018 were performed in the D experiment period, therefore both the gas puff and the beam were D. Similarly, data from the H plasmas were obtained in the H experiment period of February 8, 2019, thus H-puff and H-beam were used. On those experiment dates, the plasma facing components (PFCs) were conditioned by each fuel gas. In addition to this database, the mixed ion plasma data were obtained using the H puff in the D experiment period of December 7, 2018. Since the PFCs were maintained by the D gas, the recycling D from the walls were the dominant particle source in particular in the low electron density plasma conditions. In order to maintain the desired mixture rate, intensive discharge cleanings with H puff were performed between the shots. The shot-to-shot density scan was performed by controlling the gas puff rate with a fixed ion

purity.

Figure 2 shows the experimental condition in the database plotted in the line averaged density–D/H ratio space. Here, the D/H ratio is evaluated as $I_{D_\alpha}/(I_{D_\alpha}+I_{H_\alpha})$, where I_{D_α} and I_{H_α} are the intensity of the D_α emission and the H_α emission measured by the passive spectroscopy, respectively. Each point corresponds to one discharge, where the time-evolving data are averaged in the time period subject to the transient transport analysis of ~ 2 s. Temporal variations of the line averaged density and the D/H ratio in that time period are small, as shown by the error bars for each point. Data from different experiment dates are characterized by approximately constant D/H purities, at 89 %, 60 %, and 4 %, which we call the D plasmas, the mixed plasmas, and the H plasmas, respectively. The line averaged density is continuously scanned both in D and H plasmas in a wide range, which is sufficient to observe the density dependence in the hysteresis width [19]. In addition, four data points in low density regime are obtained from the mixed plasmas. As a representative case comparison among the D, H, and mixed plasmas, data at the line averaged density of $\sim 1.3\times10^{19}$ m^{-3} are chosen. Their shot numbers are #146822, #152229, and #147882, respectively.

4. Experimental results

4.1. Target discharge

Figure 3 shows the typical time evolution of the plasmas parameters in this experiment. The injected power of the balanced NBs is approximately 3.6 MW. Short pulse

injection of a perpendicular NB is performed as the probe beam of the charge exchange recombination spectroscopy measurement (data are not shown here). Modulation ECH (MECH) with the frequency of 23 Hz and the amplitude of ~ 1 MW launched by a single gyrotron is applied. The energy flux from electrons to ions by collision is calculated to be typically less than 10 kW, which is negligibly small. The MECH power is deposited nearly on-axis, $r_{\rm eff} < 0.1$ m, where $r_{\rm eff}$ is the effective minor radius [44]. The transient transport analysis is performed in the time period of the density flat-top, i.e., 3.8 s to 5.6 s in this discharge. The ECE measurement displays a periodic electron temperature response synchronizing the MECH pulses.

Variation of the long-time averaged mean plasma profiles in the line averaged density scan is compared in plasmas with different ion species. Figure 4 shows the electron temperature profile, the electron density profile, and the ECH deposition profile as a function of the line averaged density and the effective minor radius. When the line averaged density is decreased, the density profile changes from the hollowed profile to the peaked profile. The electron temperature profile tends to sharply peak in the low line averaged density case. In the high density cases, the ECH deposition radius moves slightly outward because the ECH ray is subject to a flection. Nevertheless, the power is still deposited within $r_{\rm eff} < 0.15$ m even in the highest density condition in this database.

4.2. Electron heat pulse transport

Radial profiles of the electron density and the electron temperature for the representative discharges for the D, H, and mixed plasmas at the line averaged density of $\sim 1.3 \times 10^{19}$ m^{-3} are shown in Figs. 5 (a) and (b). The mean profiles differ only slightly regardless of the D/H ratio, in particular where the ECH deposition is absent. Only the D plasma shows a large electron temperature gradient in the ECH deposition region of $r_{\rm eff} < 0.15$ m, which is ascribed by the electron internal transport barrier (ITB). We will show that the ITB transition condition is more tight in lighter isotope mass plasmas below.

Figures 5 (c) and (d) show the fluctuation power of the electron temperature perturbation being proportional to the square of the fluctuation amplitude and its phase difference with respect to the MECH pulse at the fundamental frequency of the modulation, 23 Hz. At the outer radii with respect to the ECH deposition location, $r_{\rm eff} > 0.15$ m, the radial derivatives of both the fluctuation power in the logarithmic scale and the phase difference are almost identical among the D, H, and mixed plasmas. Note that the vertical offset in the fluctuation power profile is likely due to imperfect matching of the density profile and ECH power absorption, and is unrelated to the transport property. As discussed in Refs. [9, 31], the heat pulse diffusion coefficient is a function of the radial gradients of the fluctuation power and the phase difference when the electron thermal transport can be approximated by the local model. Differences in the electron thermal transport property in the D, H, and mixed plasmas are invisible

where the ECH deposition is absent in the conventional local point of view. Note that the local thermal transport coefficients are shown to be insufficient to fully express the electron heat pulse propagation in LHD [28, 30].

In order to compare the electron thermal transport properties in D, H, and mixed plasmas more in detail, the heat flux evolution is derived using Eq. (1) with the measured electron temperature response and the calculated ECH deposition profile. The obtained heat flux is plotted as a function of the local electron temperature gradient as shown in the flux–gradient diagram in Fig. 6. The trajectories in the flux–gradient relation when the MECH is on and off clearly differ thus demonstrating the apparent input power dependence of the heat flux and making the hysteresis loop. The finite hysteresis widths in the D, H, and mixed plasmas seem to be identical. While, there are noticeable difference in the modulation amplitude in the electron temperature gradient, which will be discussed below.

Figures 7 (a)-(c) show the line averaged density dependence of the radial profile of the hysteresis width in the D, H, and mixed plasmas. The hysteresis width monotonically decreases as the measurement radius is apart from the ECH deposition radius. In addition, the hysteresis width decreases as the line averaged density increases, as reported in [19]. For the quantitative comparison of the hysteresis width, the line averaged density dependence of the hysteresis widths at $r_{\mathrm{eff}} = 0.14$ m, 0.20 m, and 0.26 m are plotted in Figs. 7 (d)-(f). All three plasmas with different isotope mass show a similar decreasing trend of the hysteresis width with the increasing line averaged

density at different radii. There is no significant difference in hysteresis widths exceeding the scatter of the points due to experimental errors in the D, H, and mixed plasmas.

On the contrary to the hysteresis width, there is a noticeable isotope mass dependence in the modulation amplitude in the electron temperature gradient $-\delta\nabla T_{\mathrm{e}}$ as pointed out in Fig. 6. The line averaged density dependence of $-\delta\nabla T_{\mathrm{e}}$ is shown in Fig. 8 (a). In the higher density range, $-\delta\nabla T_{\mathrm{e}}$ is mostly insensitive to the line averaged density. However, when the line averaged density is decreased below a threshold level, $-\delta\nabla T_{\mathrm{e}}$ drastically and monotonically raises. Deducing from the clear discontinuous nature of $-\delta\nabla T_{\mathrm{e}}$ evolution, it is considered that the electron temperature ITB is formed in the lower line averaged density discharges. The threshold line averaged density is clearly higher for the D plasma case at $\bar{n}_{\mathrm{e}} \sim 1.6 \times 10^{19}$ m^{-3} compared to the H plasma case at $\bar{n}_{\mathrm{e}} \sim 1.2 \times 10^{19}$ m^{-3}. A similar isotope mass dependence in the ITB threshold density is also seen in the ion temperature ITB dynamics as shown in [33].

As discussed above, the hysteresis widths do not depend on the isotope mass of the plasma. Therefore, the isotope effect in the ITB threshold density should be accounted for by the slow time scale transport dynamics according to Eq. (2) and Fig. 1. We derive the line averaged density dependence of the slow time scale diffusivity. Figure 8 (b) shows the line averaged density dependences of the peak-to-peak heat flux modulation amplitude normalized by the local electron density $\delta q_{\mathrm{ECH}}/n_{\mathrm{e}}$ and the hysteresis width $\delta q_{\mathrm{ECH}}/n_{\mathrm{e}}$. Their difference, i.e., the heat flux driven by the local electron temperature gradient at a slow time scale, is shown in Fig. 8 (c). It is shown that the heat flux driven

by the local gradient gradually increases as the line averaged density decreases, and no discontinuity is seen. The slow time scale diffusivity $\chi_{\rm e}^{\rm Slow}$ defined by Eq. (3) is exhibited in Fig. 8 (d). When the plasma is in the L-mode state in high density discharges, both $\chi_{\rm e}^{\rm Slow}$ in D and H plasmas are scaled by $\propto \bar{n}_{\rm e}^{-1.2}$. The negative exponent on the line averaged density is suggestive of the density stability effect in the confinement scaling [37]. As the density decreases, $\chi_{\rm e}^{\rm Slow}$ drops off from the $\bar{n}_{\rm e}^{-1.2}$ trend, which triggers the ITB formation. This transition in the $\chi_{\rm e}^{\rm Slow}$ trend in D plasmas occurs at the higher density level than that in H plasmas. The ITB transition in stellarator devices is primarily ascribed to be the neoclassical radial electric field transition [32]. It is deduced that the neoclassical root transition occurs in a higher density range in D plasmas, which plausibly explains the isotope mass dependence in the transition density threshold.

5. Discussion

According to Refs. [25, 26, 27], the transport hysteresis is considered to be due to the immediate response of turbulence amplitude to the increased heat input. In that model, the fluctuation amplitude at the saturation level is predicted as

$$I = \frac{I_0}{1 - \gamma_{\rm h}\chi_0^{-1}k_\perp^{-2}}, \tag{4}$$

where I_0 is the fluctuation amplitude without considering the direct heating effect, χ_0 is the turbulent diffusion coefficient in the L-mode, $k_\perp$ is the wavenumber of fluctuation that is of interest, and

$$\gamma_{\rm h} \equiv \frac{\partial P_{\rm ECH}}{\partial p_{\rm e}} \tag{5}$$

is the magnitude of the direct influence of the heating source on the fluctuation amplitude. The turbulence fluctuation is amplified when the denominator of the term in the r.h.s. in Eq. (4) is smaller than unity. The time scale of the amplification can be the ECH power absorption time, which is much faster than that of the fluctuation growth by the local gradient increase.

If one takes the transport hysteresis into account, the inverse trend of the confinement isotope effect with respect to the Bohm/gyro-Bohm prediction can be explained as follows. Bohm or gyro-Bohm scaling gives χ_0 being proportional to the ion mass. Since larger χ_0 provides a larger denominator in Eq. (4), a smaller hysteresis is expected in the heavier isotope mass. A jump in the flux–gradient relation in the hysteresis trajectory behaves to reduce the achievable temperature gradient at a fixed heat input. Therefore, a smaller hysteresis with heavier hydrogen isotope mass is favorable for obtaining a better confinement, which is an explanation of the transport isotope effect.

However, the present observation in LHD shows no isotope mass dependence of the hysteresis width in the D, H, and mixed plasmas. This observation implies that the turbulent diffusion coefficient χ_0 does not have an isotope mass dependence. According to Ref. [5], global confinement times of D and H plasmas scale similarly, which supports this implication. The isotope effect in the ITB formation is therefore considered to be not due to the turbulence property itself, but due to the ambient radial electric field condition.

Note that Eq. (4) is one of the possible models for explaining the isotope effect in the hysteresis response of the transient electron thermal transport. For steady state plasmas, other possible mechanisms were discussed, including the zonal flow effects, [45, 46, 47], the electromagnetic turbulence effect [47], the trapped electron mode effect [46], the energetic ion effect [48], and others. Application of these models for the transient plasma response with some modifications is one of the interesting direction for future study.

6. Summary

In this study, we performed a comprehensive comparison of the transport hysteresis width in deuterium (D) plasmas, hydrogen (H) plasmas, and D-H mixed plasmas. The core focused modulation ECH was applied as the heat source perturbation, and the heat flux was evaluated using the energy conservation equation with the measured electron temperature response and the ECH deposition profile calculated by the ray-tracing scheme. Systematic density scan in plasmas with different ion mass revealed that there was no significant isotope effect in their hysteresis width. It was found that plasmas with heavier isotope mass can easily form electron ITBs. As the hysteresis width was insensitive to the isotope mass, the classical part of the diffusivity was considered to be essential for the isotope effect in the ITB formation.

Acknowledgments

The authors acknowledge all the members of the LHD Experiment Group for their assistance. The authors also thank Professor S. Sakakibara for strong support and S. Satake for useful discussions. This work is partly supported by the National Institute for Fusion Science grants (17KLPH031 and ULHH033) and by the Grant-in-Aid for Scientific Research of JSPS (17K14898).

References

[1] M Bessenrodt-Weberpals, F Wagner, O Gehre, L Giannone, J V Hofmann, A Kallenbach, K McCormick, V Mertens, H D Murmann, F Ryter, *et al* 1993 *Nucl. Fusion* **33** 1205

[2] J G Cordey, B Balet, D V Bartlett, R V Budny, J P Christiansen, G D Conway, L-G Eriksson, G M Fishpool, C W Gowers, J C M De Haas, *et al* 1999 *Nucl. Fusion* **39** 301

[3] R J Hawryluk 1998 *Rev. Mod. Phys.* **70** 537

[4] C F Maggi, H Weisen, J C Hillesheim, A Chankin, E Delabie, L Horvath, F Auriemma, IS Carvalho, G Corrigan, J Flanagan, *et al* 2017 *Plasma Phys. Control. Fusion* **60** 014045

[5] H Yamada, K Tanaka, R Seki, C Suzuki, K Ida, K Fujii, M Goto, S Murakami, M Osakabe, T Tokuzawa, *et al* 2019 *Phys. Rev. Lett.* **123** 185001

[6] F W Perkins, Cris W Barnes, D W Johnson, S D Scott, M C Zarnstorff, M G Bell, R E Bell, C E Bush, B Grek, K W Hill, *et al* 1993 *Phys. Fluids B* **5** 477

[7] C C Petty, T C Luce, K H Burrell, S C Chiu, J S Degrassie, C B Forest, P Gohil, C M Greenfield, R J Groebner, R W Harvey, *et al* 1995 *Phys. Plasmas* **2** 2342

[8] G Manfredi and M Ottaviani 1997 *Phys. Rev. Lett.* **79** 4190

[9] A Jacchia, P Mantica, F De Luca, and G Gorini 1991 *Phys. Fluids B* **3** 3033

[10] N J Lopes Cardozo 1995 *Plasma Phys. Control. Fusion* **37** 799

[11] F Ryter, R Dux, P Mantica, and T Tala 2010 *Plasma Phys. Control. Fusion* **52** 124043

[12] F Ryter, F Imbeaux, F Leuterer, H-U Fahrbach, W Suttrop, and ASDEX Upgrade Team 2001 *Phys. Rev. Lett.* **86** 5498

[13] J C DeBoo, C C Petty, A E White, K H Burrell, E J Doyle, J C Hillesheim, C Holland, G R McKee, T L Rhodes, L Schmitz, *et al* 2012 *Phys. Plasmas* **19** 082518

[14] J D Callen and G L Jahns 1977 *Phys. Rev. Lett.* **38** 491

[15] E D Fredrickson, K McGuire, A Cavallo, R Budny, A Janos, D Monticello, Y Nagayama, W Park, G Taylor, and M C Zarnstorff 1990 *Phys. Rev. Lett.* **65** 2869

[16] U Stroth, L Giannone, H J Hartfuss, *et al* 1996 *Plasma Phys. Control. Fusion* **38** 611

[17] K W Gentle, M E Austin, J C DeBoo, T C Luce, and C C Petty 2006 *Phys. Plasmas* **13** 012311

[18] S Inagaki, T Tokuzawa, N Tamura, S-I Itoh, T Kobayashi, K Ida, T Shimozuma, S Kubo, K Tanaka, T Ido, *et al* 2013 *Nucl. Fusion* **53** 113006

[19] T Kobayashi, K Ida, T Ii Tsujimura, S Inagaki, T Tokuzawa, H Tsuchiya, N Tamura, H Igami, Y Yoshimura, S-I Itoh, *et al* 2018 *Nucl. Fusion* **58** 126031

[20] M W Kissick, E D Fredrickson, J D Callen, C E Bush, Z. Chang, P C Efthimion, R A Hulse, D K Mansfield, H K Park, J F Schivell, *et al* 1994 *Nucl. Fusion* **34** 349

[21] K W Gentle, W L Rowan, R V Bravenec, G Cima, T P Crowley, H Gasquet, G A Hallock, J Heard, A Ouroua, P E Phillips, D W Ross, P M Schoch, and C Watts 1995 *Phys. Rev. Lett.* **74** 3620

[22] N Tamura, S Inagaki, K Tanaka, C Michael, T Tokuzawa, T Shimozuma, S Kubo, R Sakamoto, K Ida, K Itoh, *et al* 2007 *Nucl. Fusion* **47** 449

[23] K Ida, Z Shi, HJ Sun, S Inagaki, K Kamiya, JE Rice, N Tamura, PH Diamond, G Dif-Pradalier, XL Zou, *et al* 2015 *Nucl. Fusion* **55** 013022

[24] K Itoh, S-I Itoh, K Ida, S Inagaki, Y Kamada, K Kamiya, JQ Dong, C Hidalgo, T Evans, WH Ko, *et al* 2017 *Nucl. Fusion* **57** 102021

[25] S-I Itoh and K Itoh 2012 *Sci. Rep.* **2** 860

[26] S-I Itoh and K Itoh 2013 *Nucl. Fusion* **53** 073035

[27] S-I Itoh, K Itoh, and S Inagaki 2016 *Nucl. Fusion* **57** 022003

[28] S Inagaki, S-I Itoh, K Itoh, N Kasuya, T Kobayashi, A Fujisawa, T Tokuzawa, K Ida, S Kubo, T Shimozuma, *et al* 2013 *Plasma Fusion Res.* **8** 1202173

[29] S Inagaki, S-I Itoh, K Itoh, K Ida, D López-Bruna, M A Ochand, T Estrada, B Ph van Milligen, C Hidalgo, and N Kasuya 2014 *Plasma Fusion Res.* **9** 1202052

[30] T Kobayashi, K Ida, S Inagaki, H Tsuchiya, N Tamura, GH Choe, GS Yun, HK Park, WH Ko, TE Evans, *et al* 2017 *Nucl. Fusion* **57** 076013

[31] T Kobayashi, K Itoh, K Ida, S Inagaki, and S-I Itoh 2017 *J. Phys. Soc. Jpn.* **86** 074501

[32] K Ida, T Shimozuma, H Funaba, K Narihara, S Kubo, S Murakami, A Wakasa, M Yokoyama, Y Takeiri, KY Watanabe, *et al* 2003 *Physical review letters* **91** 085003

[33] T Kobayashi, H Takahashi, K Nagaoka, M Sasaki, M Nakata, M Yokoyama, R Seki, M Yoshinuma, and K Ida 2019 *Sci. Rep.* **9** 1–8

[34] Sanae-I Itoh, Shigeru Inagaki, Jiaqi Dong, and Kimitaka Itoh 2016 *Plasma and Fusion Research* **11** 2503086–2503086

[35] M Van Berkel, G Vandersteen, HJ Zwart, GMD Hogeweij, J Citrin, E Westerhof, D Peumans, and MR de Baar 2018 *Nucl. Fusion* **58** 106042

[36] P N Yushmanov, T Takizuka, K S Riedel, O J W F Kardaun, J G Cordey, S M Kaye, and D E Post 1990 *Nucl. Fusion* **30** 1999

[37] H Yamada, JH Harris, Andreas Dinklage, E Ascasibar, F Sano, S Okamura, J Talmadge, U Stroth, A Kus, S Murakami, *et al* 2005 *Nucl. Fusion* **45** 1684

[38] P Rodriguez-Fernandez, A E White, N T Howard, B A Grierson, G M Staebler, J E Rice, X Yuan, N M Cao, A J Creely, M J Greenwald, *et al* 2018 *Phys. Rev. Lett.* **120** 075001

[39] P Rodriguez-Fernandez, A E White, N T Howard, B A Grierson, L Zeng, X Yuan, G M Staebler, M E Austin, T Odstrcil, T L Rhodes, *et al* 2019 *Phys. Plasmas* **26** 062503

[40] C Angioni, E Fable, F Ryter, P Rodriguez-Fernandez, T Pütterich, and the ASDEX Upgrade Team 2019 *Nucl. Fusion* **59** 106007

[41] H Tsuchiya, Y Nagayama, K Kawahata, S Inagaki, S Kubo, *et al* 2011 *Plasma Fusion Res.* **6** 2402114

[42] I Yamada, K Narihara, H Funaba, T Minami, H Hayashi, T Kohmoto, and LHD Experiment Group 2010 *Fusion Sci. Tech.* **58** 345

[43] T Ii Tsujimura, S Kubo, H Takahashi, R Makino, R Seki, Y Yoshimura, H Igami, T Shimozuma, K Ida, C Suzuki, *et al* 2015 *Nucl. Fusion* **55** 123019

[44] C Suzuki, K Ida, Y Suzuki, M Yoshida, M Emoto, and M Yokoyama 2012 *Plasma Phys. Control. Fusion* **55** 014016

[45] T S Hahm, Lu Wang, W X Wang, E S Yoon, and F X Duthoit 2013 *Nucl. Fusion* **53** 072002

[46] M Nakata, M Nunami, H Sugama, and T-H Watanabe 2017 *Phys. Rev. Lett.* **118** 165002

[47] J Garcia, T Görler, F Jenko, and G Giruzzi 2016 *Nucl. Fusion* **57** 014007

[48] N Bonanomi, I Casiraghi, P Mantica, C Challis, E Delabie, E Fable, D Gallart, C Giroud, E Lerche, P Lomas, *et al* 2019 *Nucl. Fusion* **59** 096030

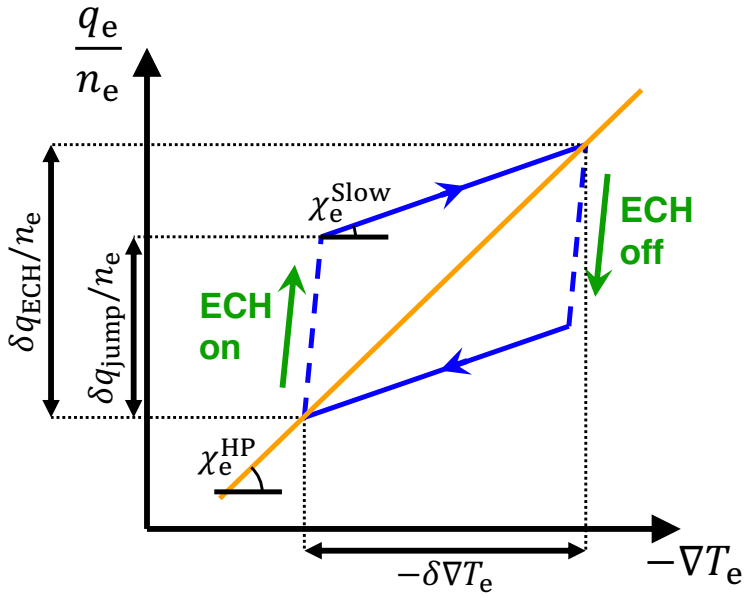

Figure 1. Schematic of the flux-gradient relation when the transport hysteresis is present.

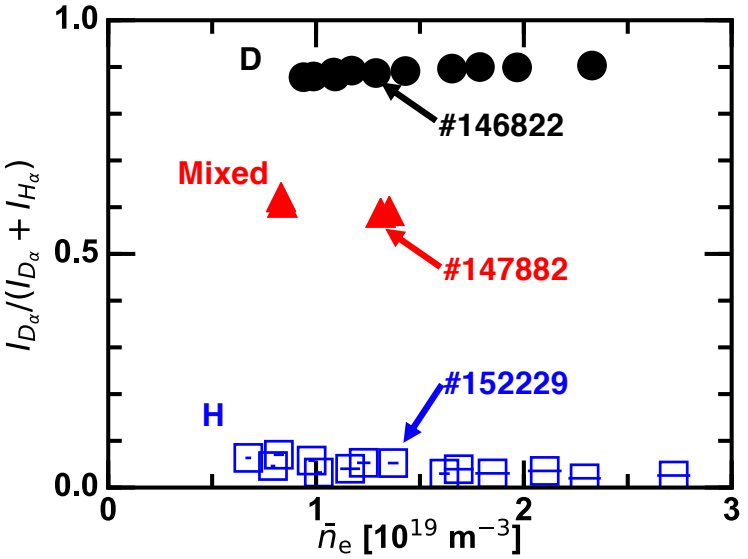

Figure 2. Experimental parameter map in the line averaged density–D/H ratio space for D, Mixed, and H plasmas. The D/H ratio is given as $I_{D_\alpha}/(I_{D_\alpha}+I_{H_\alpha})$, where I_{D_α} and I_{H_α} are the intensity of the D_α emission and the H_α emission measured by a passive spectroscopy, respectively.

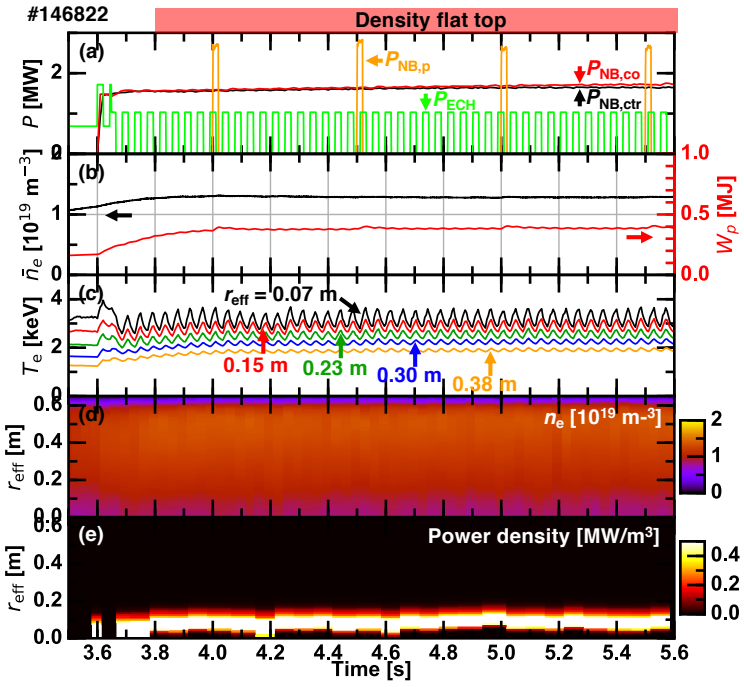

Figure 3. Time evolutions of (a) heating power, (b) line averaged density and diamagnetic plasma stored energy, (c) electron temperature, (d) electron density profile, and (e) ECH absorption profile.

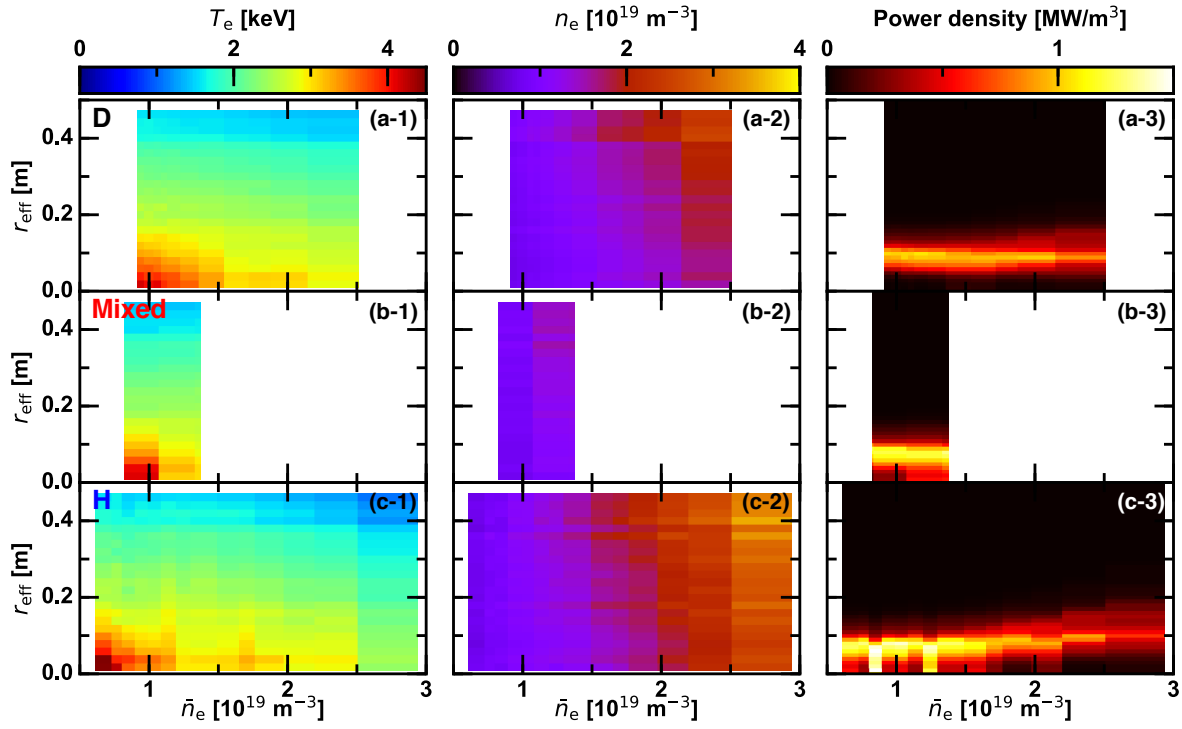

Figure 4. Line averaged density dependence of radial profiles of electron temperature (first column), electron density (second column), ECH absorption (third column) averaged in the overall analysis time period for (a) D, (b) Mixed, and (c) H plasmas.

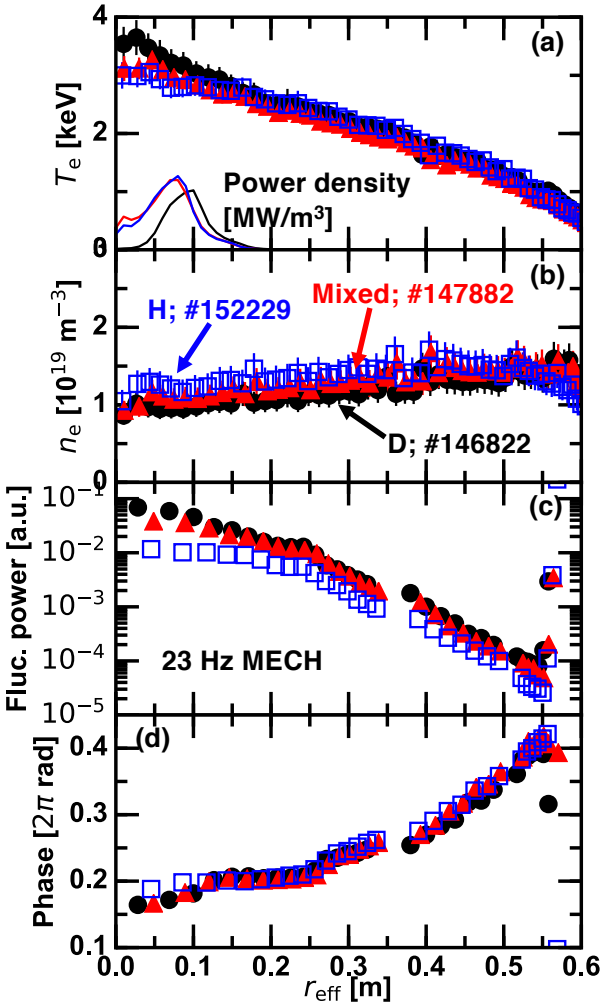

Figure 5. Radial profiles of (a) electron temperature profile and ECH power density, (b) electron density profile, and (c,d) fluctuation power being proportional to the square of the fluctuation amplitude and phase of electron temperature modulation at 23 Hz.

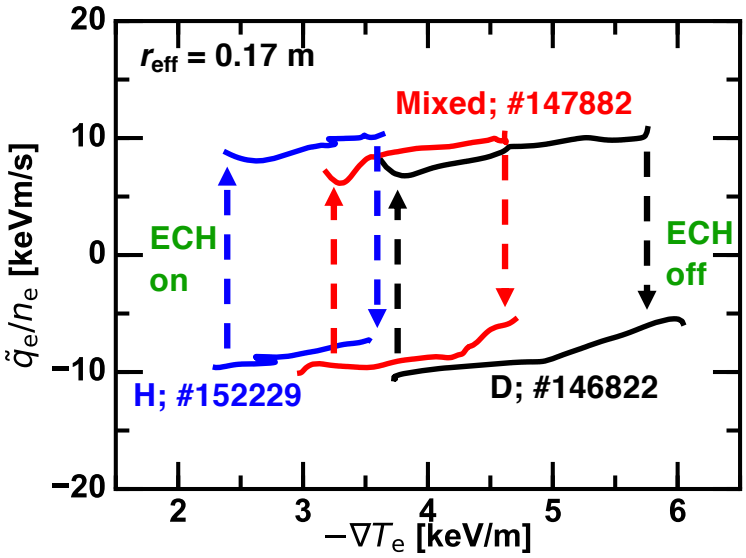

Figure 6. Trajectory of time evolution during the MECH in the flux–gradient diagram.

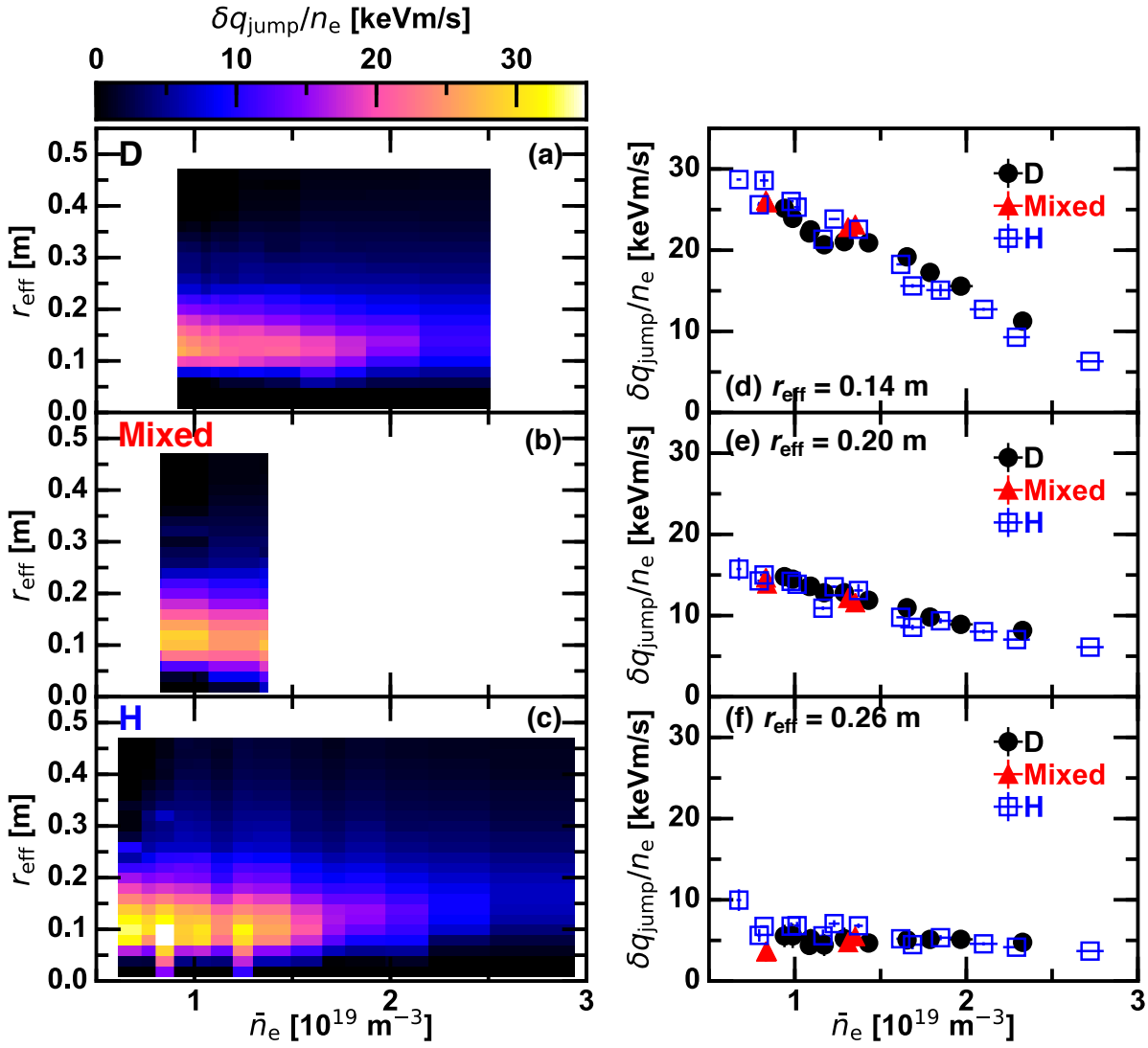

Figure 7. (Left column) Radial profile of the hysteresis width as a function of the line averaged density for (a) D, (b) Mixed, and (c) H plasmas, and (Right column) radial profile of the hysteresis width at (d) $r_{\rm eff} = 0.14$ m, (e) 0.20 m, and (f) 0.26 m.

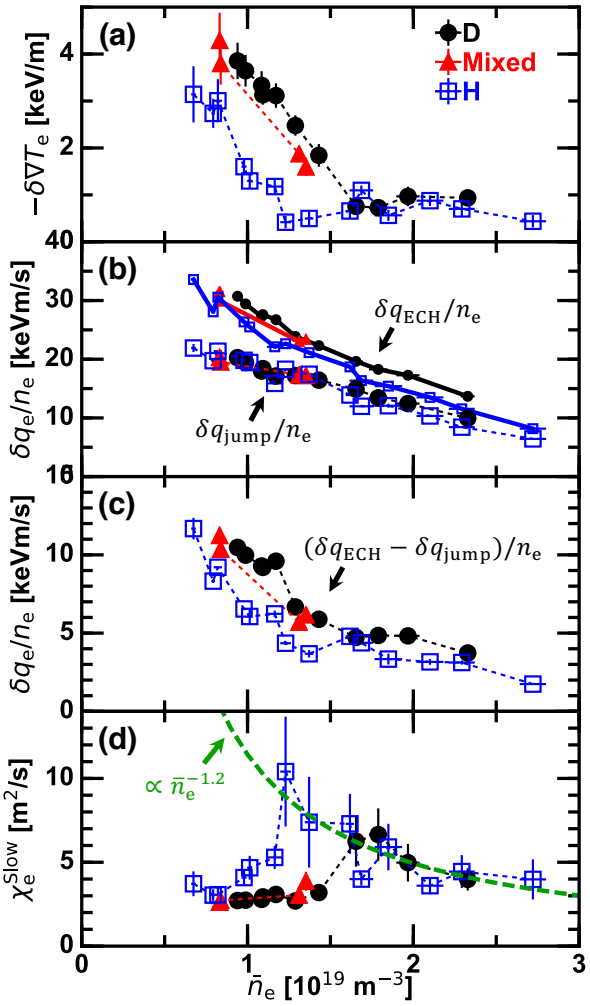

Figure 8. Line averaged density dependence of (a) the amplitude in electron temperature gradient modulation, (b) the hysteresis width δq_{jump} and peak-to-peak heat flux modulation amplitude δq_{ECH} normalized by the electron density n_{e}, (c) $(\delta q_{\mathrm{ECH}} - \delta q_{\mathrm{jump}})/n_{\mathrm{e}}$, and (d) the slow time scale diffusivity.